RJTF Mach 8 Testing of a Scramjet Engine Model of a Contraction Ratio of 8.3 with a Strut *

Takeshi KANDA[*1] Kenji KUDO[*1] Muneo IZUMIKAWA[*1]
Noboru SAKURANAKA[*2] Fumiei ONO[*1] and Shigeru SATOH[*1]

ABSTRACT

In order to improve combustion performance in a hydrogen-fueled scramjet research engine model for the Mach 8 flight condition, a thick strut was attached and the contraction ratio was increased to 8.3. According to the result of the gas-sampling at the exit of the model, a combustion efficiency of 90% was attained for the fuel flow rate $\phi = 0.8$. Normal fuel injection into the low-velocity region on the top wall, in which the recovery temperature was high, was found to be effective for ignition. The high pressure in the combustor caused by the thick strut was also found to be effective for combustion. The thrust increase from the no-fueled condition was 420 N for $\phi = 1.2$. The relatively low thrust level was caused by the Rayleigh heating loss and the base drag of the strut. Small amounts of fuel injection upstream of the step changed the combustion condition significantly, however controlled engine operation was difficult to achieve. Parallel fuel injection resulted in very poor combustion for this engine model.

Keywords: scramjet, strut

概　　要

ラムジェットエンジン試験設備(RJTF)におけるマッハ８条件でのスクラムジェットエンジン模型の燃焼性能を改善するために、幅 46mm のストラットを新規に取り付け収縮比を 8.3 に上げて試験を行った。エンジン出口でのガス採取結果によると、当量比 0.8 条件で燃焼効率は約 90% であった。回復温度の高い天板上の低速域への燃料垂直噴射が、着火に対して有効であり、ストラットによる昇圧が燃焼に対して有効であることがわかった。気流状態からの推力増分は当量比 1.2 条件で 420N であった。低推力レベルであった原因は、高マッハ数の拡大部での燃焼による高い Rayleigh 総圧損失と、ストラットでの大きなベース抗力である。ステップ上流からの少量の燃料噴射により燃焼状態は大きく変化した。燃料を平行噴射した場合の燃焼による推力増分は僅かであった。

NOMENCLATURE AND ABBREVIATION

C.C. : constant duct part of the combustor
D.C. : divergent duct part of the combustor
FMS : force measurement system
h : step height
Is : isolator
L.I. : long isolator
P_w : wall pressure
P_1 : nominal static pressure at the exit of the Mach 6.7 nozzle, pressure upstream of the shock train
P_2 : increased pressure by combustion at the end of the shock train
S.I. : short isolator
x_c : combustion position in the 1-D calculation
x_1 : streamwise distance from the leading edge of the side wall
y : vertical distance from the top wall
z : spanwise distance from center plane
ΔF : thrust increase from no-fuel condition
η_c : combustion efficiency
ϕ_{local} : local equivalence ratio
ϕ : equivalence ratio of injected hydrogen fuel

* received 22 January, 2002 **(平成 14 年 1 月 22 日受付)**
*1 Ramjet Propulsion Research Center **(ラムジェット推進研究センター)**
*2 National Space Development Agency of Japan **(宇宙開発事業団)**

INTRODUCTION

Study of an aerospace plane is being carried out to create a new transportation system for travel to and from a low earth orbit. A scramjet engine to be used in such an aerospace plane is being studied at the National Aerospace Laboratory (NAL), Kakuda Research Center. A sub-scale scramjet research engine model has been tested under Mach 4 and Mach 6 flight conditions in the Ramjet Engine Test Facility (RJTF).[1] Information from other sub-scale scramjet engine tests are not open, so the report on the tests at the RJTF is beneficial for the world-wide advance of the scramjet engine. Not only the data on the engine performance, but also many important features of the scramjet engine and the test facility were found from the tests. For example, the interaction between components affected startability of the inlet.[2] Two combustion modes were observed, and the one with a high combustion efficiency was designated as the intensive combustion mode.[3] Effect of the two air-heating methods, i.e., the vitiation heating and the storage-heating, on combustion condition was clarified.[4] Characteristics of the liquid-hydrogen cooling were also investigated.[5]

Under the Mach 8 flight condition, the sub-scale engine tests were also conducted. The Mach number and the enthalpy of the tests are the typical operating conditions of the scramjet engine. In the first series of the tests, the geometrical contraction ratio of the model was three, significantly lower than that of the design configuration, with the result that only slight thrust was produced.[6] In the second series, the engine followed the design configuration such that it had a strut and a geometrical contraction ratio was five. That strut is designated as the standard strut here. The engine produced lager thrust and auto-ignition was attained. However, a large amount of fuel ϕ =2.3 was required to produce the thrust increase of 250 N from the no-fueled condition.[7]

In the present third series, a thick strut was attached to the engine in order to improve combustion performance. This modification was expected to decelerate the air, enhance the mixing, and increase the pressure. The tests showed larger pressure increase by combustion, good mixing condition, high combustion efficiencies, but low thrust increase from the no-fueled condition. In the present paper, first, the test condition and the principal test results are presented briefly. Then discussions and analyses on the combustion condition and the thrust level follows. They will be a good help to design and modify following scramjet engines and combined-cycle engines.

EXPERIMENTAL APPARATUS AND METHODS

Test facility

The RJTF is equipped with a high-temperature and high-pressure air supply system and a vacuum ejection system. The Mach number at the exit of the facility nozzle was 6.73. The total temperature and the total pressure of the air were 2600K and 10.0MPa, respectively. They correspond to flight conditions at Mach 8 with a flight dynamic pressure of 26 kPa. The relatively low dynamic pressure was due to the facility capacity. Compressed air was heated by a ceramic storage heater and subsequently heated by a vitiation air heater. At the nominal operation, the flow rates of air, hydrogen and oxygen for the vitiation heater were 6.16 $kg \cdot s^{-1}$, 0.181 $kg \cdot s^{-1}$ and 2.16 $kg \cdot s^{-1}$, respectively. The vitiated air contained 21% oxygen and 27% water in volume fraction. The supersonic facility nozzle had exit dimensions of 51cm by 51cm. The nominal static pressure at the exit of the nozzle was 1.6kPa. The boundary layer thickness was 90mm at the engine entrance, according to pitot pressure measurements.[8] The inner surface of the top wall of the engine model coincided with that of the Mach 6.73 nozzle in order to ingest the boundary layer, simulating the entrance conditions of the engine of the aerospace plane.

Engine model

Figure 1 shows a schematic diagram of the water-cooled engine model. The top wall was at y=0 mm and the cowl inner surface was at y=250 mm. The swept angle of the side wall and the strut was 45°. The half wedge angle of 6° of the thick strut was the same as that of the standard strut used in the second series of the Mach 8 tests[7] and in Mach 6 tests.[9] The new, thick strut had to locate on the top wall between the inlet and C.C. and the strut had a wide base area due to the restriction of attachment. The strut was expected to improve the combustion condition, but was not to increase the thrust significantly due to an

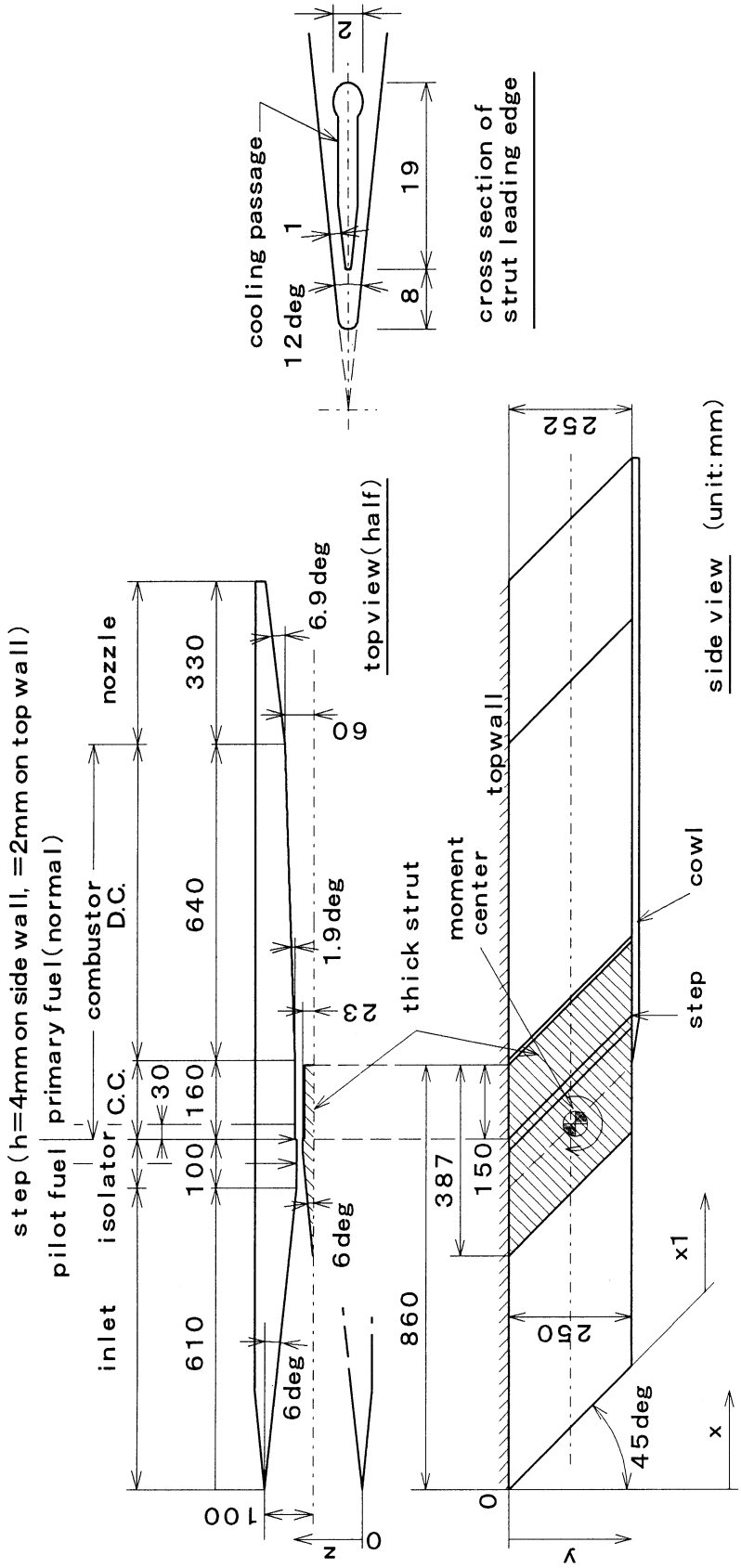

Fig. 1 Schematic of the water-cooled scramjet engine model with a strut.

anticipated, large base drag.

The parallel part of the side wall commenced at $x1$ = 609.8 mm. The geometrical contraction ratio including the strut was 5.00 and the ratio without the strut was 2.86 at $x1$ = 609.8 mm. The projected cross section at the entrance of the engine, i.e., 200 mm × 250 mm, was used as a reference area here. The leading edge of the cowl also located at $x1$=609.8 mm. The parallel part of the thick strut commenced at $x1$=685.9 mm. The gap between the side wall and the strut was 12 mm, and the geometrical contraction ratio took maximum value of 8.33 here. There was a backward-facing step at the junction of the isolator and the combustor for isolation of the pressure increase in the combustor and for flame-holding. Its height was 4 mm on the side walls and on the strut, and 2 mm on the top wall. The location of the step of the thick strut was the same as that of the side walls, i.e., $x1$=709.8 mm. The gap was 20 mm between the side wall and the strut, and the geometrical contraction ratio decreased to 8.27 downstream of the steps. No fuel was injected from the strut. The strut base located 10 mm upstream of the end of the parallel part of the side wall. The geometrical contraction ratio was 2.54 just downstream of the strut base. The divergent angle of the side wall changed at $x1$=1510 mm. There the gap between the side walls was 120 mm. The geometrical contraction ratio of 0.99 at the exit of the engine was slightly smaller than unity due to the step on the top wall in the combustor.

The hydrogen fuel was injected at sonic speed normal to the side walls through 24 holes located 30 mm downstream of the step, or parallel to the side walls through 24 holes on the side-wall steps at the Mach number of 2.9. The throat diameters of the normal injectors and the parallel injectors were 1.5 mm, and the exit diameter of the parallel injectors was 3.0 mm. The total temperature of the fuel was approximately 280 K, and the total pressure of the fuel varied up to 3.5 MPa, according to the fuel flow rate. Supplementary fuel for flame holding at the step, which is designated as the pilot fuel here, was supplied with sonic speed through 94 holes on the side walls 50 mm upstream of the step, the diameter of each being 0.5 mm. Fuel flow rates were measured by metering orifices. The model had no igniter because an auto-ignition was confirmed in the previous Mach 8 tests.[7] The fuel flow rate at the stoichiometric condition was 47 $g \cdot s^{-1}$. It was calculated with the assumption that the mass capture ratio was 0.85 from a CFD simulation of the present tests.[10] The fuel condition in each test is represented by the test number and a letter, e.g., #17a, #17e, etc.

The normal fuel injectors were designed, based on the experimental results of the supplementary tests at NAL.[11] In the tests, the normally-injected fuel jets interacted with the boundary layer behind the backward-facing step, and large separation region was created between the jets and the step. The interaction caused higher combustion efficiency and larger penetration of fuel, also in the tests at the RJTF.[3] In the design procedure of the engine used at the RJTF, the mechanism was not clear sufficiently. Thus, because of the long distance between the step and the injectors, the interaction was hard to be achieved and the penetration of the fuel was small in the engine.

The engine wall was made of copper. The engine components were individually cooled by water: (1) the leading edge of the inlet, (2) the inlet, (3) the top walls of the isolator and C.C., (4) the side walls of the isolator and C.C., (5) the cowl, (6) D.C., (7) the nozzle, and (8) the leading edge of the strut. The cooling channel of the leading edge of the strut is shown in Fig. 1. Because only the leading edge was cooled in the strut, the test duration time was limited to 15 seconds.

Measurements

(1) *Wall pressure and heat flux*

In the present paper, the wall pressure is non-dimensionalized with the nominal static pressure at the exit of the Mach 6.73 nozzle. In the figures discussed below, the pressure on the top wall was measured along the center line of the channel. The pressure distributions on the side wall are shown at three positions;

(1) P_w near the top wall, i.e., at y=10 mm in the inlet and at y=45 mm downstream of the inlet. This position is designated as 'Side wall near the top wall' in the figures.
(2) P_w at y=125 mm. This position is designated as 'Side wall at the mid height.'
(3) P_w near the cowl, i.e., at y=240 mm from the inlet to the end of C.C. and at y=210 mm in

D.C. and the nozzle. This position is designated as 'Side wall near the cowl.'

The wall pressure positions are not arranged at the specified y coordinates, because of the arrangement of the cooling water passages. The measurement error of the nondimensionalized wall pressure was ±0.3 in the inlet, ±0.06 in the isolator and C.C., and ±1 in D.C. and nozzle.

Heat flux was estimated from the rate of the temperature change of the cooling water and the water flow rate. The error of heat fluxes was ±0.15 MW.

(2) *Force and momentum*

Thrust and lift were measured by a floating frame force measurement system (FMS). The error of forces was ±50N. The lift was positive for a vehicle-up or engine-up direction, i.e., against the y-direction in Fig. 1. Pitching moment was also measured. The center of the moment center was at x = 741.43 mm and y = 135.8 mm. The moment was positive for a vehicle-nose-up direction, as shown in Fig. 1. The measured thrust/drag by FMS contained additional drag which should not be included in the net thrust estimation. Therefore, the increase of the thrust caused by the combustion from that in the no-fueled condition is evaluated and shown in figures and listed in tables.

(3) *Gas sampling and pitot pressure measurement*

Gas sampling and pitot pressure measurement were carried out at 60 locations at the exit of the engine model using probes, each with a sampling orifice of 0.3 mm, after probe calibration.[12] With the measured results by the gas sampling and the pitot pressure measurement, the distributions of equivalence ratio, mass flux, and the combustion efficiency were attained. The error of the combustion efficiency was ±0.05, including the error of measuring systems and the quenching effect in the sampling probe. The error of the equivalence ratio and that of the pitot pressure were ±0.03 each.

1-D calculation

A 1-D calculation was conducted to estimate the flow condition in the engine model. The model was used in the previous investigation on the test results at the RJTF.[3] Assumptions and calculation conditions were as follows.

(1) The effect of the swept angle was ignored, and the distance from the leading edge was used when the calculated results were compared with the experimental data.
(2) The air and the combustion gas were equilibrium flows through the engine.
(3) The inlet kinetic energy efficiency was 0.99 from the pressure distribution in the inlet of the present model. The mass capture ratio was 0.85 according to the estimation by CFD.
(4) The specified part of hydrogen burned quickly in a stoichiometric condition at the specified location. The ratio of the reacted hydrogen represented combustion efficiency here. The residual hydrogen mixed with the residual air.
(5) The combustion gas and the non-combusted mixture expanded isentropically in D.C.
(6) Boundary layer was turbulent throughout the engine. The friction coefficient was calculated with the formula of van Driest.[13]

EXPERIMENTAL RESULTS

Combustion with normal fuel injection

In the present tests, a high combustion efficiency was measured with the normal fuel injection, but the thrust increase was small. In this chapter, principal results are presented. First, pictures of the operating conditions of the engine model and a chart of the thrust vs. the fuel flow rate are shown to grasp the outline of the test results. Then the details of the engine operating conditions were presented with the distributions of the wall pressure, the map of the local combustion efficiencies and others.

(A) *Engine operating conditions*

Figures 2 (a) and (b) show the engine operating conditions of the thick strut model with the normal fuel injection. The number represents the test number, and the alphabet represents the fuel supply condition in each test. The engine was mounted on FMS upside down. The air flowed from the left. In the starting condition, the combustion gas flowed out from the engine. In the unstarting condition, the combustion gas spilled out from the inlet.

(B) *Thrust increase, lift and pitching moment*

Figures 3 (a), (b) and (c) show the thrust increase by combustion from the no-fueled condition, the lift, and the pitching moment. When the normal fuel injection was employed, the thrust increased approximately proportional to the fuel flow rate (●).

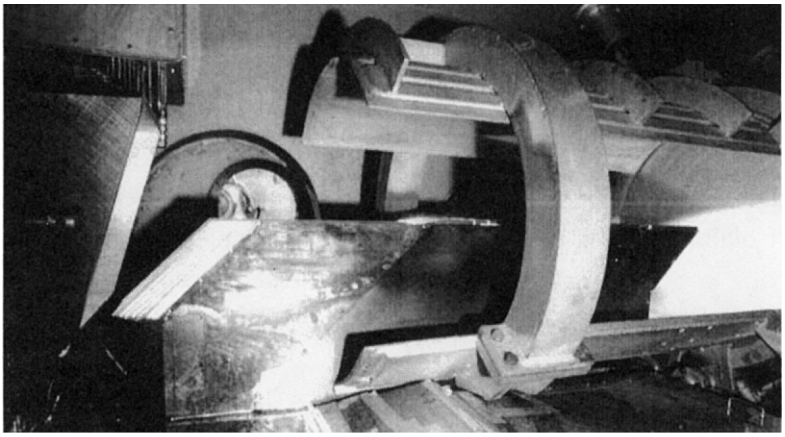

(a) Starting condition at $\phi = 0.7$ in 17e test condition.

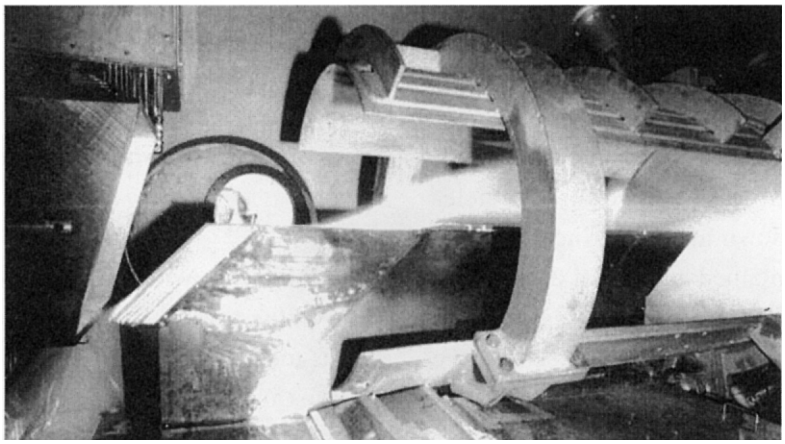

(b) Unstarting condition at $\phi = 0.8$ in 15d test condition.

Fig. 2 Engine operating condition.

When the fuel equivalence ratio was larger than 1.2, the engine fell in the unstarted condition. Between ϕ =0.8 and 1.2, there observed hysteresis between the started and the unstarted conditions. In the region from ϕ =0.8 to 1.2, when the fuel flow rate decreased in the unstarted condition during a test, the engine remained in the unstarted condition.

When the parallel fuel injection was combined with the normal fuel injection, the region of the started condition was enlarged, but the thrust level was lower than that by the normal injection (◯). The scatter of the thrust data was due to the various combinations of the injected fuel flow rates.

A drag of 780 N in the no-fueled condition was measured by FMS. The thrust by FMS includes additional drag besides the net drag. Here, the net drag is defined as a sum of the drag on the inside of the engine and that on the outer surface of the cowl, whereas the additional drag is a sum of the drag on the outer surface of the side-walls and that on the force measuring stand. According to the force measurement in the supplementary tests,[14] the net drag in the no-fueled condition was estimated to be 320N. In the condition of ϕ =1.2 by the normal fuel injection at #21b, the net thrust was estimated to be –60 N.

The lift decreased when the fuel flow rate increased in the started condition. The increase of the pressure was larger around the cowl than on the top wall in the divergent part of the combustor, which will be shown in Figs. 4. In the unstarted condition, the pressure in the inlet increased, and the lift became positive. The pitching moment, which was 600 to 800N•m^{-1} except around no-fueled condition, was higher in the started condition than in the unstarted condition. In the started condition and the unstarted

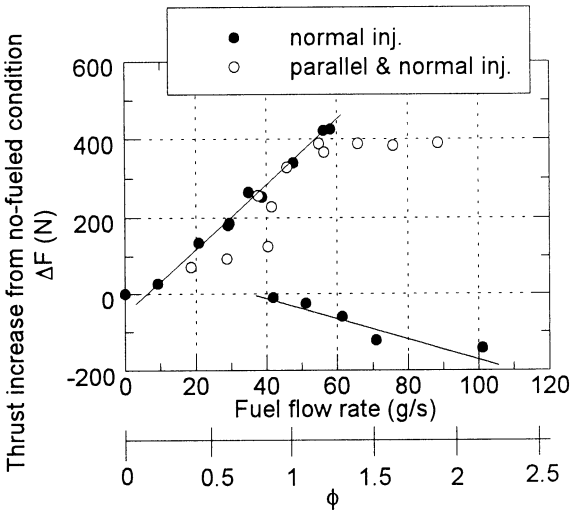

(a) Thrust increase from that in the no-fueled condition.

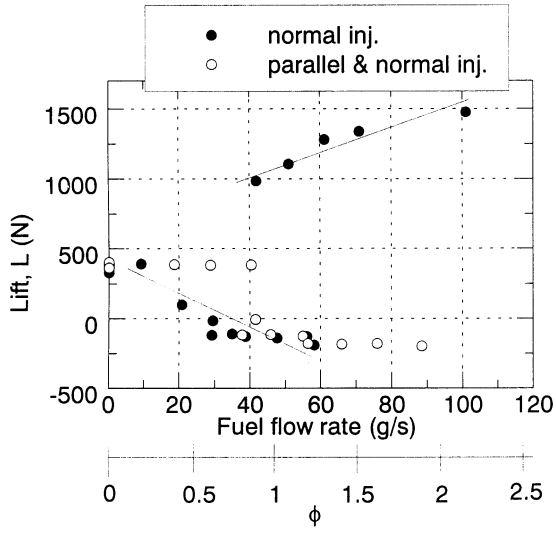

(b) Lift

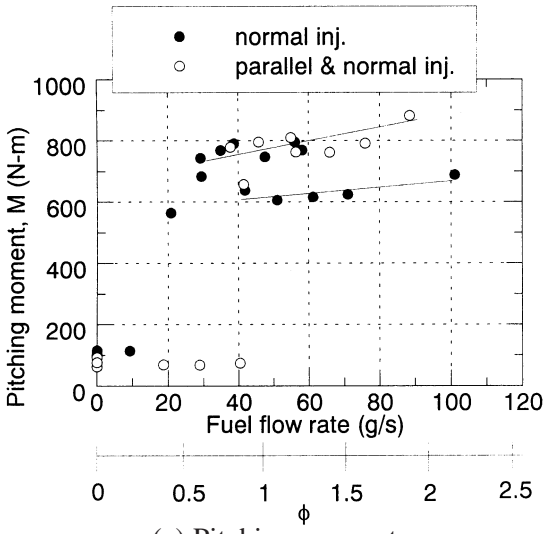

(c) Pitching moment

Fig. 3 Forces and moment measured by FMS.

condition, the pitching moment became positive, because the pressure on the cowl of the divergent part of the combustor was high in the started condition, whereas that of the inlet was high in the unstarted condition.

(C) *Wall pressure distribution*

As shown in Fig. 3, the remarkable thrust increase was attained with the normal fuel injection. Figures 4(a) to (d) show the wall pressure distributions with normal fuel injection. The fuel flow rates and the thrusts are listed in Table 1. The lower pressure on the top wall than on the side wall was caused by the airflow being turned toward the cowl by the shock wave reflections in the convergent component with the swept angle. When the fuel flow rate was increased, the wall pressure, as well as the thrust, increased.

With fuel injection, the top wall pressure increased in the isolator, i.e., upstream of the step and the fuel injectors. On the side wall near the top wall and at the mid height, the wall pressure increased downstream of the fuel injector position, and the increase became notable from $x1$ = 1000 mm in D.C. On the side wall near the cowl, the pressure around the injectors reached the rule-of-thumb for combustion of one-half an atmosphere of pressure.[15] However, there was only a small increase of the wall pressure from that in the no-fueled condition. These distributions were different from those of the intensive-combustion mode in the Mach 6 tests, in which the wall pressure significantly increased near the cowl on the side walls and also increased behind the step.[3]

The simulation result at $\phi = 0.8$ with the 1-D flow calculation is shown in Fig. 5. In the calculation, the fuel was injected normally in C.C. and burned at $x1$ = 1000mm in D.C. instantaneously. This combustion position was determined from the experimental results. The combustion efficiency was assumed to be 0.95 in the calculation. The calculated pressure distribution shows reasonably good agreement with the experimental one. The combustion efficiency at $\phi = 0.8$ was estimated to be about 0.9 in the test by the 1-D calculation. When the engine model was in the unstarted condition, the wall pressure in the inlet was higher than that in the airflow condition (Fig. 5). The side wall pressure was as high as that of the no-fueled condition downstream of the step.

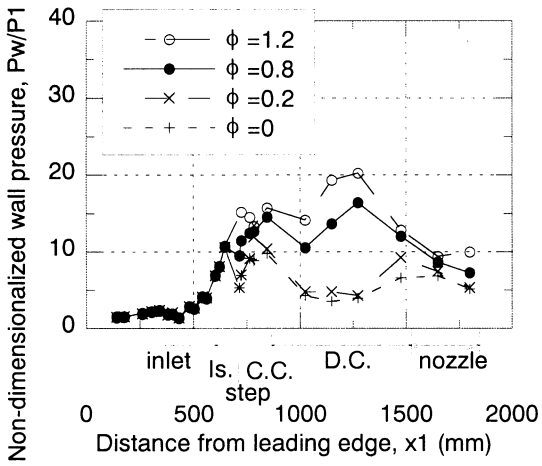

(a) Top wall.

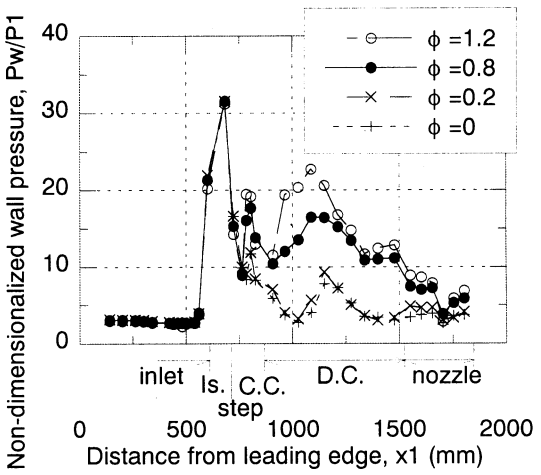

(c) Side wall at the mid height.

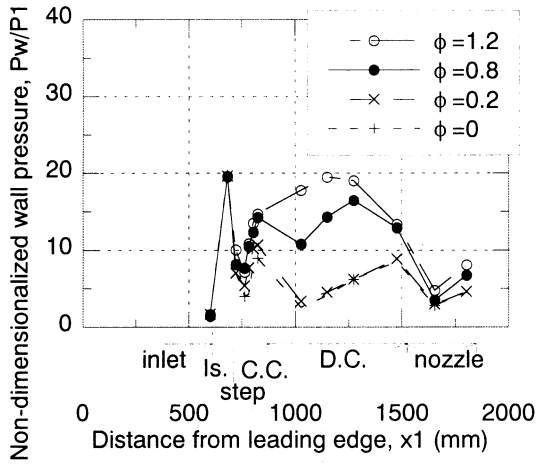

(b) Side wall near the top wall.

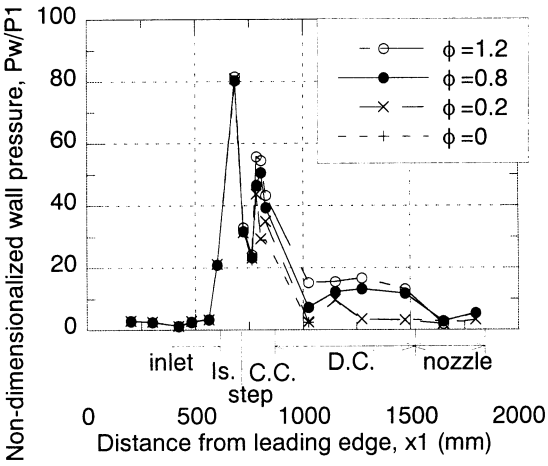

(d) Side wall near the cowl.

Fig. 4 Wall pressure distributions with normal fuel injection.

Table 1 Thrust by norml fuel injection

Test No.	Fuel flow rate ($g \cdot s^{-1}$)			Equivalence	Thrust increase from
	Normal	Parallel	Sidewall Pilot	ratio	no-fueled condition (N)
17e	38.7	0	0	0.82	253
16d	9.2	0	0	0.20	27
21b	56.1	0	0	1.19	421
15d	41.9	0	0	0.89	-10 (unstarted)
27c	60.4	0	0	1.29	2 (unstarted)

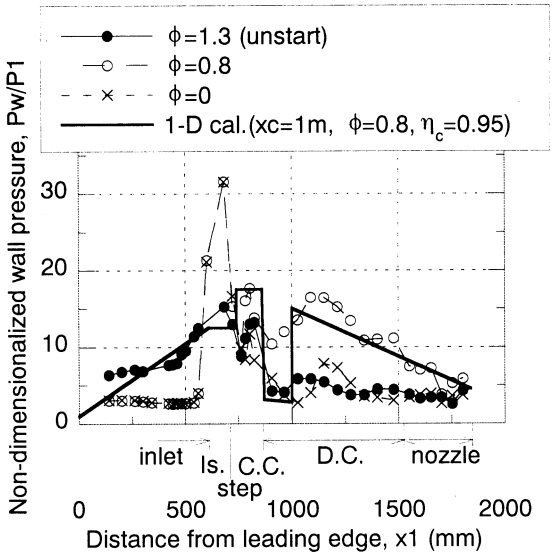

Fig. 5 The simulated wall pressure distribution by the 1-D calculation and the wall pressure distributions in the unstarted condition with normal fuel injection on the side wall at the mid height.

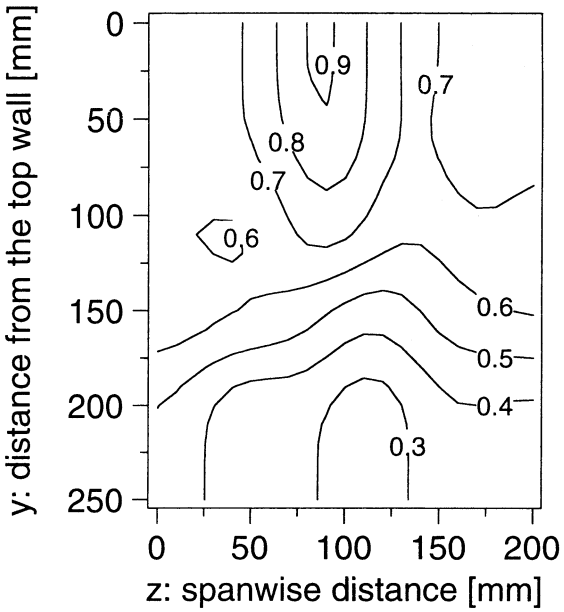

Fig. 6 Distribution of local equivalence ratio at the engine exit with fuel flow rate $\phi = 0.8$ normal injection.

(D) *Mixing and combustion efficiency*

The thrust increase was remarkable with the normal fuel injection, and the engine was in the started condition steadily below ϕ =0.8. Therefore, the gas sampling was conducted under the normal fuel injection with ϕ =0.8. Figure 6 illustrates the distribution of the local equivalence ratio of hydrogen measured at the exit of the engine on a swept-back plane. Hydrogen was concentrated in the center region around z =100 mm near the top wall. The distribution of the equivalence ratio shows a different feature from that in the Mach 6 tests. In the intensive-combustion mode of the Mach 6 tests, rich hydrogen regions were formed in the corners between the top wall and the side walls.[9] On the whole, however, hydrogen spread well in the spanwise direction. In the vertical direction, hydrogen was concentrated on and near the top wall, as well as in the Mach 6 tests.[4]

The contour lines of local combustion efficiency for the tests described above are shown in Fig. 7. A narrow region with combustion efficiency lower than 85% was found at the center of the top wall. However, in most regions, the combustion efficiencies were higher than 85% with the average about 90%. A general tendency for the lower combustion efficiency to be located in the richer region was noted in the present testing.

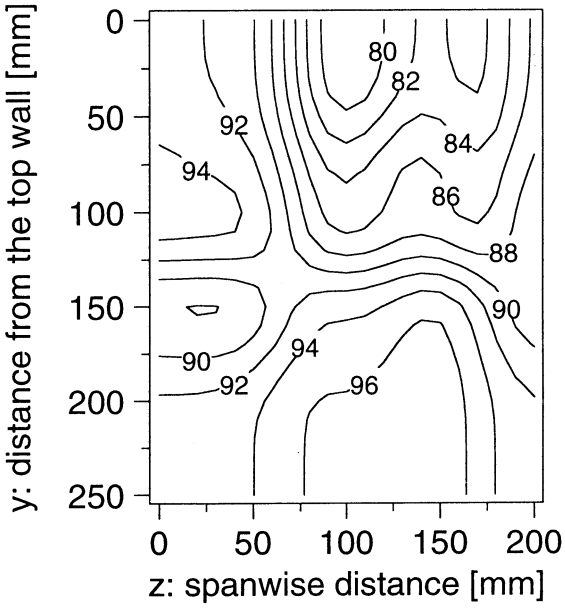

Fig. 7 Contour lines of local combustion efficiency at the engine exit with fuel flow rate ϕ= 0.8 normal injection.

(E) *Heat flux*

The heat flux experienced by the isolator and C.C. was 2 MW•m^{-2} in both the no-fuel condition and the combustion condition. The fact indicates that the fuel did not burn in C.C. significantly. The heat flux in D.C. was about 0.8 MW•m^{-2} with ϕ=0.8, whereas it was about 0.3 MW•m^{-2} in the no-fueled condition. The change was larger than the error ±0.15 MW. This

indicates that the combustion occurred primarily in D.C. In the unstarted condition, the heat flux in the inlet slightly increased from 0.2 MW•m^{-2} for the started condition to 0.4 MW•m^{-2}, while decreasing in D.C. to 0.4 MW•m^{-2}. This feature was similar to that seen in the Mach 6 tests.[3)]

Combustion with other fuel injection methods

When the fuel was injected from the parallel fuel injectors, little thrust was produced as shown in Table 2 for the case #26e. The slight increase of thrust was mainly caused by the jet thrust associated with the fuel injection nozzles. The thrust by the tangentially-injected fuel jet was estimated to be 90 N at the fuel flow rate of 40g•s^{-1}, and it was 70% of the measured thrust increase at #26e. When large amounts of fuel was supplied from both the normal fuel injectors and the parallel fuel injectors, the engine remained in the started condition, as seen in the #26f and in Fig. 3.

When the pilot fuel injection upstream of the step was used with the normal injection downstream of the step, the unstarted condition occurred in the #20c test (Table 2). When the larger amount of fuel was supplied from the normal fuel injectors alone, the engine was in the started condition in the #21b test as shown in Table 1. When a small amount of fuel was injected from the pilot fuel injectors with the parallel fuel injection, the engine produced higher thrust (#28f). Use of the pilot fuel injection increased thrust. However, control of the combustion condition by use of the pilot fuel injection was difficult in the present testing, because the mechanism of the combustion enhancement was not yet clarified and the results were highly sensitive to the pilot flow rate.

Table 2 Effects of parallel fuel injection and pilot fuel injection

Test No.	Fuel flow rate (g·s^{-1})			Equivalence	Thrust increase from
	Normal	Parallel	Sidewall Pilot	ratio	no-fueled condition (N)
26e	0	40.4	0	0.86	124
26f	48.1	40.4	0	1.88	389
20c	38.7	0	11.3	1.06	-73 (unstarted)
28f	0	28.4	3.8	0.69	202

According to Reference 16, when there was the secondary injection upstream of the primary injection, the boundary layer was disturbed and the penetration height of the primary jet increased. This disturbance mechanism might have improved the combustion condition in the present tests. The blowing parameter was 10 with the injection of the pilot fuel at 8 g•s^{-1}, i.e., ϕ=0.17. In the Mach 6 tests, intensive combustion was attained by the addition of the pilot fuel injection of 8.4 g•s^{-1}.(ϕ = 0.06) to the normal injection of 36 g•s^{-1} (ϕ = 0.25).[3)] The blowing parameter was also 10 in the test.

DISCUSSION

First, the discussions on the combustion mode and the effect of the air heating mode on the engine performance are presented to clarify the engine operating condition of the present tests. Then, the reasons and the mechanisms of the test results are discussed, i.e., the characteristic distribution of the hydrogen fuel, the high combustion efficiency and the low thrust level.

Mixing-controlled combustion in Mach 8 tests

In unsteady flow consisting of turbulent eddies, lean and rich mixtures are collected alternately by a

gas-sampling probe. These mixtures contain excess oxygen or hydrogen even if the deficient reactant is completely consumed, i.e., if the instantaneous combustion efficiency is unity. They are eventually mixed in the sampling bottle and indicate a lower time-averaged combustion efficiency. This effect becomes pronounced in near-stoichiometric mixtures. If the combustion is rate-controlled by chemical reaction rates, the combustion efficiency should not decrease at the stoichiometric condition. Regarding the present experimental results as shown in Figs. 6 and 7, a low combustion efficiency of around 80% was observed for a near-stoichiometric condition of f_{local} = 0.9. This indicates that the engine model operated in the mixing-controlled regime in the Mach 8 flight condition tests. It implies that dependence of the engine performance on air heating modes[4] may not have been strong in the tests.

Distribution of hydrogen fuel

In the vertical direction, hydrogen was concentrated on and near the top wall. One of the reasons of this distribution of hydrogen in the vertical direction was the non-uniformity of the mass flux of the air entering the combustor. According to measurement, the flux of the air was about 1.5 times larger near the cowl than near the top wall, resulting in small concentrations of hydrogen. The air turned toward the cowl in the inlet and the isolator, and the flux was large around the cowl. Another reason was the flow deflection toward the top wall through expansion fans from the ridges with a swept-back angle, especially the fan from the rear corner of the strut. The velocity component vertical to the ridge increases through the expansion fan, whereas the tangential component to the ridge is conserved. The mechanism of the flow direction change resembles that in the inlet with a swept-back angle. The injected hydrogen was probably carried by the deflected airflow in D.C.

The local equivalence ratios show relatively uniform distribution in the spanwise direction, even far from the fuel injectors. The penetration height of the normally-injected fuel was small as described previously and was estimated to be 3 mm by the formula of Reference 16 at the condition of fuel flow rate ϕ = 0.8, the total pressure of the fuel 2.1MPa and the ratio of the dynamic pressure of the fuel to that of the airflow 3.5. The gap between the strut and the side wall was 20 mm, much larger than the penetration length. Therefore, the concentration toward the center in the spanwise direction was not caused by the increase of the penetration of the fuel.

One of the possible mechanisms for the observed hydrogen spread is turning of the flows through expansion fan from the strut. The airflow spread to the center through the expansion fan from the rear corner of the strut. The normally injected hydrogen fuel turned and conveyed by the airflow, resulting in the spread of the hydrogen. If the fuel is accelerated to the velocity of the airflow after expansion to the pressure in C.C., the Mach number of the hydrogen fuel is estimated to be 2.5, which is lower than 5 of the airflow in the combustor. Here, the nominal velocity of airflow in the engine is 2000 $m \cdot s^{-1}$, which was estimated from the wall pressure. The airflow turned approximately 20° and the pressure decreased through the expansion fan.[17] If the fuel had expanded to the decreased pressure, the turning angle of the hydrogen fuel would have been about 30°. There must be intensive interaction between the fuel and the air, and the interaction promoted mixing.

A slight concentration of the hydrogen downstream the strut was observed in the Mach 6 tests.[9] In the Mach 6 tests, the difference of the Mach numbers between the fuel hydrogen and the airflow was small, and the interaction must have been weak. In the Mach 6 tests with the short strut, which was attached on the top wall and its height was 1/5 of the engine, the region with the above interaction was restricted, and mixing was not promoted.

Ignition and combustion in Mach 8 flow condition

On the top wall, there was the thick boundary layer, which had the height of about 40% of the engine. The airflow was decelerated through the many shock wave reflections in the inlet and the isolator and the low-velocity region on the top wall was thickened. In addition, the airflow in the convergent section with the swept angle was turned toward the cowl and this turning thickened the low-velocity region on the top wall. Such thickening was observed in the Mach 4 test condition.[18] The height of the subsonic region on the top wall was estimated to be about 30 mm from the CFD result.[10] As described in the previous

section, the engine operated in the mixing-controlled combustion regime in the Mach 8 test condition, i.e., chemical reactions progressed relatively fast. The ignition time at a static pressure of 15 kPa and a total temperature of 2600 K was estimated to be 2×10^{-5} seconds for the thick-strut model.[19] Here, the ignition time was defined as the time required to raise 5% of total temperature increase by combustion. The ignition distance was thus 40 mm for a flow velocity of 2000 m•s^{-1}, which is the nominal velocity of airflow in the engine. Temperature as high as the recovery temperature was required for ignition. Sufficient high temperature was attained in the low-velocity region on the top wall. The first normal fuel injection port was at y=5 mm from the top wall. From it, the fuel was injected into the low-velocity region. Because the top wall pressure began to increase in the isolator, ignition and subsequent combustion are believed to have initiated in the low-velocity region around the step and the fuel injectors. Such low-velocity region did not exist other than on the top wall in the present engine. In the Mach 6 tests with the intensive combustion mode, the low-velocity region also exist around the cowl surface. This difference of position of the low-velocity region made the difference of the combustion condition between the Mach 6 and the Mach 8 tests.

The combustion time scale and the combustion length were estimated to be 5×10^{-4} seconds and 1 m in C.C. in the thick-strut model and 3×10^{-3} seconds and 6 m in the no-strut model. Here, the combustion time scale is defined as the time required to raise the temperature from 5% to 95% of the equilibrium temperature rise. The combustion length is the product of the combustion time and the nominal velocity of airflow in C.C. of 2000 m•s^{-1}. The combustion process is strongly affected by pressure. Though the pressure level was much lower than that in the isolator, the pressure level in D.C. higher in the thick-strut model than in the no-strut model or the standard-strut model with the contraction ratio of 5. This pressure level worked well to shorten the combustion time scale.

The above estimated combustion lengths were made for the mixture. The combustion actually completed further downstream than at the estimated length, because of fuel-air mixing. In the experiments, the combustion process seemed to be completed rapidly, even though in basic turbulent mixing layers, mixing is slow.[20] In the thick-strut model, around the top wall, the mixing progressed rapidly in the low-velocity region. The mechanism of hydrogen spread through the expansion fan and the deflections to and from the top wall also promoted mixing of the hydrogen with the air and thus shortened the combustion time. The reacted gas would be also carried by the spreading mechanism of the hydrogen. The carried combustion gas induced the subsequent reaction far from the low-velocity region on the top wall.

The base region of the strut was also the low-velocity region in the combustor. However, the region did not directly contribute to enhanced combustion in the present tests. The measured pressure for the strut base at y=125 mm did not change during a test in the started condition. As mentioned before, the penetration of the fuel jet injected from the side walls was small and the fuel jet did not reach the base other than on the top wall. In addition, base pressure is significantly low and it is not favorable to burning.

The first parallel-injection port was in the low-velocity region at y=15 mm from the top wall. The injectant had a velocity of approximately 2000 m•s^{-1} at the parallel fuel injector exit such that not much of it remained in the low-velocity region. The velocity was similar to that of the airflow, and any mixing of airflow with the fuel was weak.

Reason for the low thrust

In the present tests, a high combustion efficiency was achieved, but the thrust increase was small. The specific impulse was 2000 m•s^{-1} with the estimated net thrust of 100 N at ϕ = 1.2. One reason for the small achieved thrust was the large base drag of the strut. An increase in pressure was observed far downstream of the strut except on the top wall. The pressure on the base plane of the strut was low, and the resultant drag of the overall strut was large. Another reason for the small thrust was the Rayleigh heating loss due to combustion in the expanded, high-Mach-number flow. The increased pressure caused by the addition of heat decreases with the increase of the Mach number of the flow. Because the possible region of ignition was only on the top wall in the present engine, the radicals would be carried from

that region to the downstream in the engine and the combustion succeeded in D.C, where the Mach number was rather high. Thus the heating loss became large in this engine.

The thrust of the engine model can possibly be increased by modification of the strut base shape and by moving the combustion position upstream. According to the 1-D calculation, when there is combustion at the injector position with the combustion efficiency of 95% at ϕ =0.8, the calculated net thrust will be 800 N and the specific impulse will be 16000 m•s^{-1}. To attain such operation, creation of the low-velocity region on the side walls is necessary for short ignition time and enhanced mixing. Avoiding the unstarted condition discussed below is also necessary.

As shown in Table 2, a low level of thrust was produced by the parallel fuel injection. When the parallel fuel injection was combined with the normal fuel injection, probably, the fuel from the parallel fuel injectors hardly reacted. Therefore, the started condition was held and the thrust did not further increase in the region of the large equivalence ratio.

Unstarted condition

The combustion in C.C. near the injectors will be necessary for decreasing the heating loss and increasing the thrust. However, it was pointed out that the combustion in C.C. would cause the unstarted condition in the engine with the standard strut.[7] In the present engine with the thick strut, the Mach number in the isolator was about 4 according to the 1-D calculation and the measured wall pressure. The separation pressure[21] in the isolator was about 130kPa. When there is combustion in C.C., the increased pressure due to the combustion at the combustion efficiency of 0.95 will be 150 kPa at ϕ = 1.0, according to the 1-D calculation. The pressure due to the combustion is higher than the separation pressure. Therefore, there will be a shock train in the isolator. The shock train is anticipated to become long on the top wall, where there is the low-velocity region.

The shock train length in the duct was estimated by an empirical formula,[22] in which momentum thickness is required. The momentum thickness of 40 mm at the entrance of the engine was used here. The thickness was 15 mm in the Mach 4 test condition and 30 mm in the Mach 6 test condition. In the estimation by the formula, the duct height was replaced by the gap of the flow channel in the engine. Measured pressures on the top wall at the entrance of the isolator, P_1, were used for the upstream values of the shock trains, and estimated results are shown in Figure 8 with origin at the step. The increased pressure by combustion, P_2, was assigned at the step. Shock train length is the length between the position of P_2 and the initial position of the shock train. The experimental results are also shown in the figure. Measured maximum top wall pressures within the started condition are plotted as P_2 against the length of the isolator. Here, the started condition is defined that combustion does not affect the pressure distribution in the inlet. In the limit of the started condition, the shock train would start at the entrance of the isolator, and the length of the shock train in the experiments was almost the same as that of the isolator. In some tests, a long isolator (L.I.) was used. Its length was 200 mm, longer than that of the short isolator of the present model (S.I.), whose length was 100 mm. In the Mach 4 tests, there was no strut. In the Mach 6 tests, two kinds of struts were used; the 1/5 strut whose height was 1/5 of the engine height[3] and the standard strut.[9] In the Mach 4 test conditions, the model fell into the unstarted condition due to the development of the separation on the top wall.[2] The estimated results agreed with the experimental

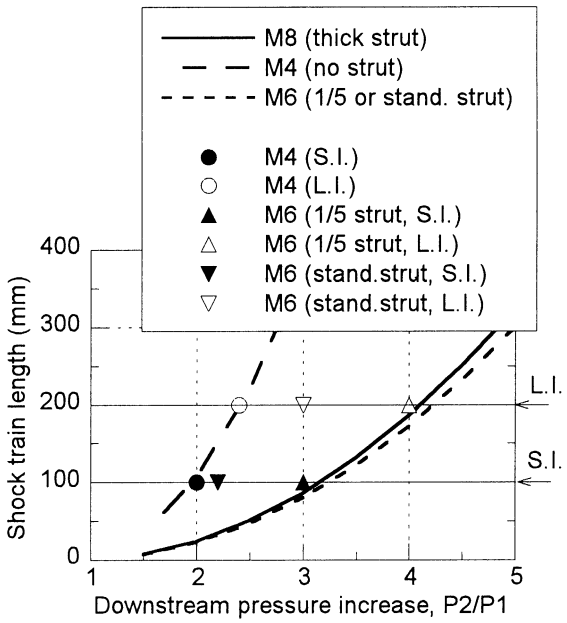

Fig. 8 Estimated shock train lengths in the isolator for Mach 4, 6 and 8 test conditions.

observations. In the Mach 6 tests, the unstarted condition initiated with a lower pressure increase than in the calculation. It was caused by the fact that the engine fell into the unstarted condition due to the separation on the cowl in the Mach 6 tests.[3] In the present Mach 8 tests, when there is combustion with ϕ =1.0 and combustion efficiency of 95% in C.C., the average pressure is estimated to be 150 kPa. Because the experimental top wall pressure in the airflow condition was low around 15 kPa at the step position, the ratio of the pressure increase will be large to 10. According to the estimation results of the shock train, an isolator of approximately 1 m will be necessary for the pressure increase. The thick strut thickened the low-velocity region on the top wall, and the region was favorable to ignition. However, the thick low-velocity region increased the upstream-influence distance and the length of the shock train. The low-pressure level on the top wall was also a negative factor for the started condition. To shorten the shock train, the low-velocity region should be thinned, or the ratio of the pressure increase should be decreased on the top wall in the isolator.

The Kantrowitz-Donaldson's criterion is well known for the maximum allowable contraction ratio to the started condition.[23] Once the started condition is attained, the contraction ratio can become larger. This is an example for the hysteresis between the started condition and the unstarted condition of the inlet, and it is for a supersonic decelerating duct flow. In the present tests, the pressure increase in the combustor induced the unstarted condition, and a large separation on the top in the inlet. The hysteresis between the started condition and the unstarted condition was due to this large separation in the inlet. Once the separation appeared, the flow structure with the large separation was held to lower equivalence ratio, as shown in Fig. 3(a).

CONCLUDING REMARKS

In order to improve combustion condition, a scramjet engine model with a thick-strut was tested under the Mach 8 flight condition of the RJTF. The engine geometrical contraction ratio was 8.3. The following points were clarified from the tests and the discussions.

(1) The hydrogen fuel burned well in the thick-strut engine model with a combustion efficiency of 90% at the flow rate of ϕ = 0.8.

(2) Ignition condition was easily attained in the hot, low-velocity region on the top wall in the combustor. The region was due to the thick boundary layer and the turning of the airflow toward the cowl. High pressure in the combustor by the thick strut was found to be effective for combustion.

(3) The unstarted condition was caused by the thick, low-velocity region and the low-pressure level on the top wall.

(4) The thrust increase from the no-fueled condition was 420 N at ϕ =1.2. The small thrust was due to the Rayleigh heating loss and the base drag of the strut. The large heating loss was due to the fact that the ignition region was limited only on the top wall in the engine.

(5) With parallel fuel injection, fuel did not react significantly. However, pilot fuel injection upstream of the step changed the combustion conditions.

ACKNOWLEDGEMENTS

The authors wish to thank the members of the scramjet research group of NAL for cooperation in testing, data processing, and discussion. The present study was conducted as a part of the program of NAL-Mitsubishi Heavy Industries LTD. cooperative research.

REFERENCES

1) N. Yatsuyanagi, N. Chinzei, T. Mitani, Y. Wakamatsu, G. Masuya, S. Iwagami, M. Endo and G. Hanus; Ramjet Engine Test Facility (RJTF) in NAL-KRC, Japan, AIAA Paper 98-1511 (1998/4).

2) T. Sunami, N. Sakuranaka, K. Tani, T. Hiraiwa and T. Shimura; Mach 4 Tests of a Scramjet Engine-Effect of Isolator, Proceedings of 13th International Symposium on Air Breathing Engines (1997) pp. 615-625, AIAA.

3) T. Kanda, T. Hiraiwa, T. Mitani, S. Tomioka and N. Chinzei; Mach 6 Testing of a Scramjet Engine Model, Journal of Propulsion and Power, Vol. 13, No. 4 (1997) pp. 543-551.

4) T. Mitani, T. Hiraiwa, S. Sato, S. Tomioka, T. Kanda and K. Tani; Comparison of Scramjet

Engine Performance in Mach 6 Vitiated and Storage-Heated Air, Journal of Propulsion and Power, Vol. 13, No. 5 (1997) pp. 635-642.
5) Y. Wakamatsu, N. Chinzei, F. Ono, T. Saito, T. Kanda, S. Tomioka and N. Yatsuyanagi; Design and Preliminary Experiments of Liquid Hydrogen Cooled Scramjet Engine, The 12th International Symposium on Space Technology and Science Paper 98-a-1-27 (1998/5).
6) T. Saito, Y. Wakamatsu, T. Mitani, N. Chinzei, T. Shimura and T. Kanda; Mach 8 Testing of a Scramjet Engine Model, Proceedings of the 20th International Symposium on Space Technology and Science, Vol. 1 (1996) pp. 58-63, International Symposium on Space Technology and Science Committee.
7) S. Tomioka, T. Kanda, K. Tani, T. Mitani, T. Shimura and N. Chinzei; Testing of a Scramjet Engine with a Strut at Mach 8 Flight Condition, AIAA Paper 98-3134 (1998/7).
8) T. Hiraiwa, T. Mitani, M. Izumikawa and F. Ono; Calibration Studies of Nozzle Flow in Ramjet Engine Test Facility, The 12th International Symposium on Space Technology and Science Paper 96-d-14 (1996/5).
9) S. Sato, M. Izumikawa, S. Tomioka and T. Mitani; Scramjet Engine Test at Mach 6 Flight Condition, AIAA Paper 97-3021 (1997/7).
10) M. Kodera, T. Sunami and K. Nakahashi; Numerical Analysis of Scramjet Combusting Flows by Unstructured Grid Method, AIAA Paper 2000-0886 (2000/1).
11) N. Chinzei, T. Komuro, K. Kudou, A. Murakami, K. Tani, G. Masuya and Y. Wakamatsu; Effects of Injector Geometry on Scramjet Combustor Performance, Journal of Propulsion and Power, Vol. 9, No. 1 (1993) pp. 146-152.
12) T. Mitani, M. Takahashi, S. Tomioka, T. Hiraiwa and K. Tani; Analyses and Application of Gas Sampling to Scramjet Engine Testing, Journal of Propulsion and Power, Vol. 15, No. 4 (1999) pp. 572-577.
13) F.M. White; Viscous Fluid Flow (1974) pp. 632-640, McGraw-Hill.
14) T. Mitani, T. Kanda, T. Hiraiwa, Y. Igarashi and K. Nakahashi; Drag in Scramjet Engine Testing: Experimental and Computational Fluid Dynamic Studies, Journal of Propulsion and Power, Vol. 15, No. 4 (1999) pp. 578-583.
15) W.H. Heiser, D.T. Pratt, D.H. Daley and U.B. Mehta; Hypersonic Airbreathing Propulsion, AIAA Education Series (1994) pp. 233, AIAA.
16) L.S. Cohen, L.J. Coulter and W.J. Egan Jr.; Penetration and Mixing of Multiple Gas Jets Subjected to a Cross Flow, AIAA Journal, Vol. 9, No. 4 (1971) pp.718-724.
17) P.K. Chang; Separation of Flow, 1st ed. (1970) pp. 531-607, Pergamon Press.
18) M. Kodera, K. Nakahashi, T. Hiraiwa, T. Kanda and T. Mitani; Scramjet Inlet Flow Computations by Hybrid Grid Method, AIAA Paper 98-0962 (1998/1).
19) T. Mitani, N. Chinzei and T. Kanda; Reaction and Mixing-Controlled Combustion in Scramjet Engines, Journal of Propulsion and Power, Vol. 17, No. 2 (2001) pp. 308-314.
20) W.H. Heiser, D.T. Pratt, D.H. Daley and U.B. Mehta; Hypersonic Airbreathing Propulsion, AIAA Education Series (1994) pp. 280-313, AIAA.
21) E.E. Zukoski; Turbulent Boundary-Layer Separation in Front of a Forward-Facing Step, AIAA Journal, Vol. 5, No. 10 (1967) pp.1746-1753.
22) G. Sullins and G. McLafferty; Experimental Results of Shock Trains in Rectangular Ducts, AIAA Paper 92-5103 (1992/12).
23) Crocco, L., “One-Dimensional Treatment of Steady Gas Dynamics,” Fundamentals of Gas Dynamics, edited by H.W. Emmons, Princeton Univ. Press, Princeton, NJ, 1958, pp. 184-190.